International Journal of Rock Mechanics & Mining Sciences 78 (2015) 1–9

Contents lists available at ScienceDirect

International Journal of Rock Mechanics & Mining Sciences

journal homepage: www.elsevier.com/locate/ijrmms

Case study of seismic hazard assessment in underground coal mining using passive tomography

Anye Cao [a,b], Linming Dou [a,b,*], Wu Cai [a,b], Siyuan Gong [b], Sai Liu [a,b], Guangcheng Jing [a,b]

[a] Key Laboratory of Deep Coal Resource Mining, Ministry of Education of China, School of Mines, China University of Mining & Technology, Xuzhou, Jiangsu 221116, China

[b] State Key Laboratory of Coal Resource and Mine Safety, China University of Mining & Technology, Xuzhou, Jiangsu 221116, China

ARTICLE INFO

Article history:
Received 24 August 2014
Received in revised form
21 March 2015
Accepted 1 May 2015
Available online 3 June 2015

Keywords:
Passive velocity tomography
P-wave velocity
Seismic hazard
Island coalface
Overburden
Rock burst

ABSTRACT

The relation between applied stress and wave velocity is examined firstly at the laboratory-scale by using ultrasonic technique. Subsequently, an island longwall face under hard-thick strata, suffering from the threat of seismic hazards, e.g. rock burst, strong tremor, was chosen for a case study of passive velocity tomography. Based on continuous seismic monitoring during mining operation, passive tomographic imaging has been used to locate high seismic activity zones and assess seismic hazard around the face. The results show that the high velocity and velocity gradient regions correlated well with the high seismic activities occurred in future mining period. In addition, the high velocity or velocity gradient regions redistributed with the retreat of coalface and large-scale movement of key strata. Passive velocity tomography can be a promising tool to continuously monitor the relatively high stress zone or evaluate seismic hazard in underground coal mining.

1. Introduction

The safety and productivity of underground mining can be severely affected by seismic activity. Mining-induced seismic events, which are induced by sudden release of strain energy accumulated in the coal-rock mass, are associated with not only superficial structure movement triggered by stress manifestation, but also related to large geological discontinuity, affected by the extent and means of mining [1,2]. Rock bursts and strong tremors are particular cases of seismic events induced by mining activity that result in damage to underground workings or surface buildings, and in some cases, injury and loss of life [3]. In China, these dynamic hazards are encountered in many coal mines due to large-scale rupture or movement of hard strata, irregular layout of coalface, large mining depth, reaction of anomaly geological structures, etc., and become progressively more severe as the average mining depth and mining intensity increase continuously [4,5].

Anomalous information identification and mining stress analysis is the key issue to reduce and prevent the hazards. Several methods to estimate abutment pressure, detect structure defaults, and evaluate rock burst hazard around the coalface have been introduced, such as electromagnetic emission [6,7], drilling bits [8], acoustic emission [9], borehole exploration [10], and pressure sensor installation [11], etc. The conventional methods mentioned above are not sufficient to meet the needs of underground mining and engineering projects due to the shortcomings of time consuming, easy disturbance, localized monitoring range, or destructive effect in production, etc. Thus, it needs to develop a simple, rapid, and cost-effective tool for imaging locations of stress concentration zones, anomaly geological structures, or high seismic activity zones during mining operation. Microseismic monitoring has been proven as a powerful tool to quantify seismicity and can contribute valuable information for dynamic hazard evaluation [12]. In addition, as a new geophysical method, the velocity tomography has been gradually used for crack detection, geological structure exploration, stress redistribution imaging, etc. [13]. Therefore, combining the microseismic monitoring and tomography imaging, may be a better approach for seismic hazard assessment or pre-warning in coal mining.

Velocity tomography relies on the transmission of seismic waves, especially P-waves, through coal-rock mass. It can be classified as “active” and “passive” based on the type of source used [14]. Active tomography, which using explosives [15], hammer strikes [16,17], vibrations generated by shearer [18], etc., as the sources, can allow for consistent seismic ray path distribution. It is preferred to apply in the relatively accurate detection of stress distribution and hidden structure defaults in the pre-mining coalface, while the detection area usually does not exceed areas of 200 m × 200 m and is not

* Corresponding author at: Key Laboratory of Deep Coal Resource Mining, Ministry of Education of China, School of Mines, China University of Mining & Technology, Xuzhou, Jiangsu 221116, China. Tel.: +86 13952261972; fax: +86 516 83995904.
E-mail addresses: lmdou@cumt.edu.cn, lmdou@126.com (L. Dou).

http://dx.doi.org/10.1016/j.ijrmms.2015.05.001
1365-1609/

always feasible for long time-lapse investigation [14,19]. Passive tomography, which using mining-induced seismic events as the sources [14,19–23], can continuously estimate the relatively high stress or rock burst hazard during the whole mining process, and its detection area can reach to about 2000 m × 2000 m [19] if the layout density of microseismic monitoring network is high and the ray path density meets the inversion requirement.

Stress distribution in various underground structures has been imaged by passive tomography, including longwall panels, coal pillars, entries, geologic structures and discontinuities, etc. [14,22–27], while there are few examples of rock burst hazard detection using passive velocity tomography [19,20,28]. Particularly, application of passive tomography starts fairly late in China, and is mostly used in geophysical exploration [13,25] and earthquake tomography [29,30], while the application in stress distribution imaging and seismic hazard evaluation in underground mining has been seldom involved [28].

The sites chosen for this study are an underground island longwall face in Baodian Coal Mine, Yanzhou Mining Group, Shandong Province, China, where strong mining-induced tremors and rock bursts are the main safety threats in underground coal mining. The face was monitored continuously by microseismic network for 8 months. Thus, the site has considerable microseismic activities, making it ideal for passive tomographic imaging of high seismic activities during mining process.

2. Velocity tomography for seismic hazard assessment

2.1. Experimental relation between stress and wave velocity

The origins of tomography can be traced back to the X-ray discovery in 1895 by Wilhelm Conrad Roentgen [31]. Modern technology allows doctors to use X-rays to map the internal human body. Based on the same key principles, scientists have extended tomography to the geophysical field by using seismic waves [32], which is known as seismic tomography. P-wave is the first part of the seismic wave to arrive and generally the easiest to measure. Thus, the key of the seismic tomography relies on the variation of seismic waves (especially P-wave) transmitted through rock mass under stress. According to the inversion parameters of seismic wave, seismic tomography can be classified as velocity tomography and attenuation tomography [27]. In velocity tomography, the inversion parameter is the wave velocity distribution with travel time, and attenuation tomography focuses on measuring the amplitude of seismic wave to detect the absorption property of geological media. Additionally, seismic velocity tomography is classified as “active” and “passive” based on the type of source used [14].

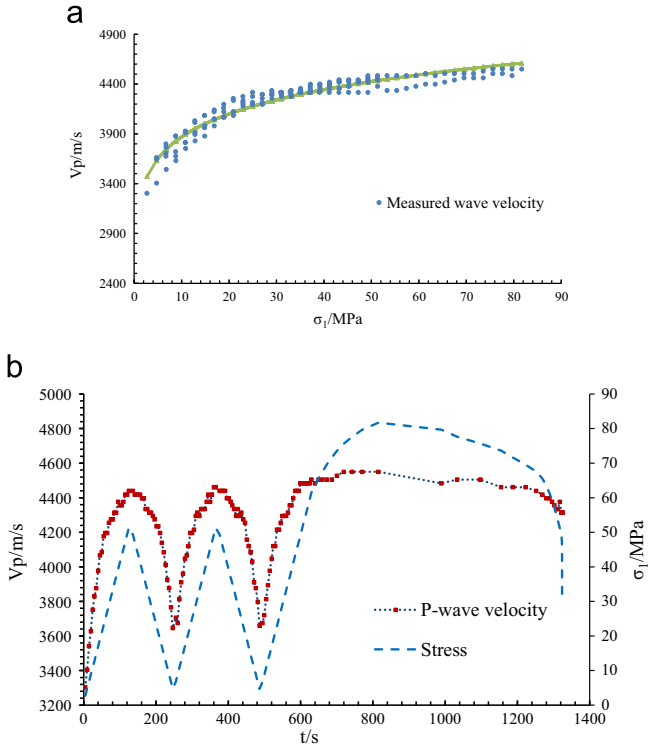

Fig. 1. Relation between stress and ultrasonic wave velocity in uniaxial loading test: (a) relation between wave velocity and stress in uniaxial compression loading and (b) relation between wave velocity and stress in uniaxial cyclic loading and unloading.

As early as in 1920s, Adams et al. found that passive tomographic imaging should be built on the close relation between elasticity modulus of rock mass and wave velocity [33]. Yale discovered that rock porosity may decrease with the increase of stress, which results in the increase of wave velocity transmitted in rock mass [34]. Meanwhile, it is found that obvious change of wave velocity always appears in the high stress stage [35], and velocity variation also correlates with the roughness of rock fracture plane [36].

To understand how velocity tomography can be applied in stress state imaging and seismic hazard assessment, and investigate the relation between seismic wave and stress, the ultrasonic wave velocities of rock samples were tested under the uniaxial compression and uniaxial cyclic loading and unloading conditions, respectively. The rock samples were collected from no. 10 Mining District of Baodian Coal Mine, and were processed to cylinders with the height of 100 mm and width of 50 mm. There are two inner-set ultrasonic sensors functioned as receiver and transmitter in the upper and lower plate of MTS815 loading system, respectively. Meanwhile, one circumferential and two axial extensometers were installed for acquiring the circumferential and axial strain data. In addition, a layer of lead foil with 0.3 mm in thickness was attached to the upper and lower surface of rock samples before the loadings, so as to obtain clearer ultrasonic signals [28]. At the loading intervals of three seconds, the transmission velocities of acoustic waves through the samples were acquired along with the stress loaded.

Fig. 1 shows the typical fitting curves of stress and ultrasonic wave (P-wave) velocity during loading process. It is found that there exists an exponential function relation between P-wave velocity and axial stress. In the uniaxial compression loading, P-wave velocity usually increases rapidly with the increase of stress at lower stress levels, and after the inelastic stage of rock samples, the increasing gradient of wave velocity slows down and gradually turns to be stable at higher stress level. In the uniaxial cyclic loading and unloading process, the stress variation correspondingly results in the change of P-wave velocity, while wave velocity changes quickly during the loading and unloading process of lower stress stages, and changes slowly in the higher stress stages.

In coal mines, the occurrence of seismic hazards, e.g. rock burst, strong tremor, is closely related to the underground in situ and mining stresses. Above results in the laboratory present that velocity tomography can be useful for inferring the stress state and redistribution in coal-rock mass. Thus, the high seismic activity zones and seismic hazards can be assessed by tomographic imaging.

2.2. Theory of velocity tomography

Tomography requires dividing the body into grid cells called pixels in two-dimensional situation, or cubes called voxels in three-dimensional situation to estimate the body characteristics in all pixels or voxels. Velocity tomography depends on the

relation that the wave velocity along a seismic ray is the ray path distance divided by the time to travel between the seismic source and receiver.

Suppose the ray path of the ith seismic wave is L_i and the travel time is T_i, thus, the time is the integral of the inverse velocity (or slowness), multiplied by the distance traveled from the source to the receiver [1,14]:

$$V = \frac{L}{T} \rightarrow VT = L \tag{1}$$

$$T_i = \int_{L_i} \frac{dL}{V(x,y,z)} = \int_{L_i} S(x,y,z)dL \tag{2}$$

$$T_i = \sum_{j=1}^{m} d_{ij} S_j \quad (i = 1, \ldots, n) \tag{3}$$

where $V(x,y,z)$ is the velocity (m/s), L_i is the ray path of the ith seismic wave (m), T_i is the travel time (s), $S(x,y,z)$ is the slowness (s/m), d_{ij} is the distance of the ith ray in the jth voxel, n is the total number of rays, m is the number of voxels.

Generally, seismic event location and subsequent ray path are calculated using an initial velocity model. However, the velocity, distance, and time in an individual voxel are not known. Thus, arranging the slowness, distance and time for each voxel into matrices, the velocity can be determined in matrix form as [14]

$$\mathbf{T} = \mathbf{DP} \rightarrow \mathbf{P} = \mathbf{D}^{-1}\mathbf{T} \tag{4}$$

where $\mathbf{T}$ is the travel time per ray matrix ($1 \times n$), $\mathbf{D}$ is the distance per ray per voxel matrix ($n \times m$), $\mathbf{P}$ is the slowness per grid cell matrix ($1 \times m$).

Matrix inversion methods are effective, but require considerable computational power for large datasets. Usually, the inverse problem is either underdetermined (more voxels than rays), or overdetermined (more rays than voxels) [14]. The most effective way to solve this problem is iterative process. Currently, the most referenced iterative methods are Algebraic Reconstructive Technique (ART) and Simultaneous Iterative Reconstructive Technique (SIRT).

2.3. Assessment model of seismic hazard

The determination of stress state and concentration degree is the basis of seismic hazard assessment during mining operation. In underground mining, there exists positive anomaly of P-wave velocity in high stress or stress concentration region, and negative anomaly of wave velocity in pressure-relief area. Positive velocity anomaly is expressed as [28,37]

$$A_n = \frac{V_p - {V_p}^a}{{V_p}^a} \tag{5}$$

where V_p is P-wave velocity of a certain point, and ${V_p}^a$ is the average velocity of the model. The relation between positive anomaly of wave velocity and stress concentration can be shown in Table 1 [37].

Moreover, underground seismic hazards are also liable to occur along the zones with high stress differences, where may exist obvious velocity gradients. VG value is used to express the variation degree of velocity gradient, and the anomaly of VG can be shown by [28]:

$$A_n = \frac{VG - VG^a}{VG^a} \tag{6}$$

where VG^a is the average value of the model. Similarly, the relation between VG anomaly of wave velocity and seismic hazard can be shown in Table 2.

Table 1
Relation between positive anomalies of wave speed and stress concentration.

Seismic risk index	Stress concentration degree	Positive velocity anomaly, A_n (%)
0	None	<5
1	Weak	5–15
2	Middle	15–25
3	Strong	>25

Table 2
Relation between VG anomaly and seismic hazard.

Seismic risk index	Stress difference degree	VG anomaly, A_n (%)
0	None	<5
1	Weak	5–15
2	Middle	15–25
3	Strong	>25

3. Site characteristics

Baodian Coal Mine, owned and operated by Yanzhou Mining Group, is located in the southwest of Shandong Province, China. Strong tremors have occurred frequently in Baodian Coal Mine, while the maximum magnitude of mining-induced tremor is up to 3.7, occurred in Longwall (LW) 10304 (a coalface in No. 10 Mining District) on 21 May, 2005, inducing all the safety valves of hydraulic supports opening, roof descending obviously, and serious vibration around the whole face. Another example, an airproof wall in the tailentry of LW2310 (a coalface in No. 2 Mining District) was destroyed seriously by the burst wave of strong tremor happened in the goafing on 6 September 2004 (seen in Fig. 2), while another four airproof wall collapse accidents happened continuously in No. 2 Mining District (head entry of LW2304, tailentry of LW2306, tailentry of LW2307, headentry of LW2307) on 29 April 2006, respectively, induced by the disturbances of strong tremors.

As shown in Fig. 3, the south side of LW10305 neighbors on the goafing of LW10306, the north side is adjacent to the goafing of LW10304, 10303, 10302 and 10301, the east side is the boundary of the minefield, while the west part neighbors on the goafing of No. 2 Mining District. Meanwhile, the east half part of LW10305 has been minded about 945 m in 2004, so the subsequent left half part, which is the research object in this paper, will form a special island mining structure surrounded by four sides mined areas due to the irrational exploitation.

Fig. 4 displays the synthesis column map of Borehole 99-1 in LW10305. Upper No. 3 Coal Seam of about 6.22 m in thickness, which is the mining coal layer of LW10305, is buried about 480 m under the surface. The main roof of about 22.64 m in thickness is mainly composed of gritstone, which is called the No. 1 inferior key stratum above the coal seam based on the key strata theory [38], while the No. 2 inferior key stratum is a siltstone stratum of about 20.07 m in thickness, approximately 113 m above the coal seam. In addition, there exists a primary key stratum (gritstone stratum) of over 200 m in thickness, approximately 135 m above the Upper No. 3 Coal Seam. During mining process, the thick and super-thick key strata overlying LW10305 and surrounding goafing areas may move together and rupture drastically, which can cause seismic hazards in the vicinity of LW10305.

Moreover, the total goafing width of LW10304, 03, 02 and 01 (about 750 m) in the north side of LW10305 is much larger than the mining depth (about 480 m) of the coal seam, which means the overburden above the goafing has caved and ruptured sufficiently. Conversely, the goafing width of LW10306 (about 200 m)

Fig. 2. Airproof wall destroyed by strong tremor happened on 6 September 2004.

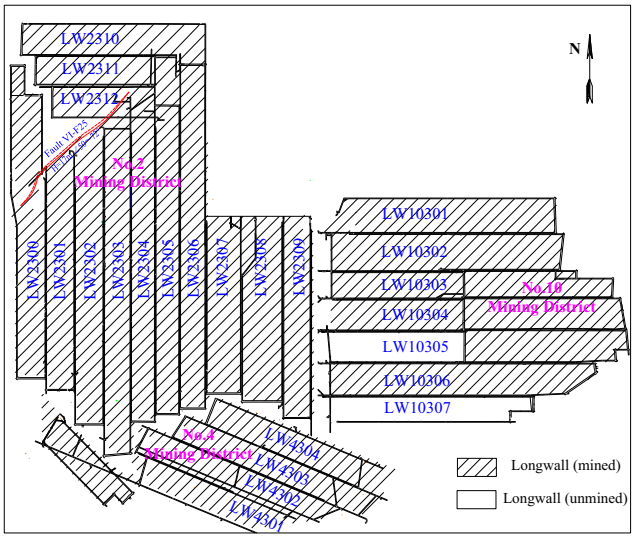

Fig. 3. Layout of LW10305 in No. 10 Mining District.

in the south side of LW10305 is much less than the mining depth of the coal seam, which means there was almost no obvious fracturing in the super-thick primary key strata because of the limited mining area. Thus, due to insufficiency mining on the side of LW10306 and sufficiency mining on the side of LW10304, LW10305 is a special island longwall face, while the fracturing structure of primary key strata can be expressed as a T-type structure in the vertical section. After LW10305 being mined, the overburden (particularly above LW10305 and 10306) may move together, especially the primary "O-X" structures in the plane view will be formed periodically [38], which will have significant effect on the stress redistribution and occurrence of strong tremors, even rock bursts during mining operation. Meanwhile, considering that there exist weak interlayers within the super-thick key stratum, the stratum may rupture in layers. The simple overburden fracturing structure above LW10305 can be seen in Fig. 5.

4. Case study

4.1. Data acquisition

Microseismic monitoring in mines allows for calculating seismic event location, energy, and source mechanisms, inferring mining stress state, and evaluating rock burst hazard, etc. Since 15 July 2008, the microseismic monitoring system called "SOS" that developed by Central Mining Institute (GIG) of Poland has been installed in Baodian Coal Mine. Fig. 6 displays the longwall geometry and relative geophone locations, there are nine geophones (blue circles)

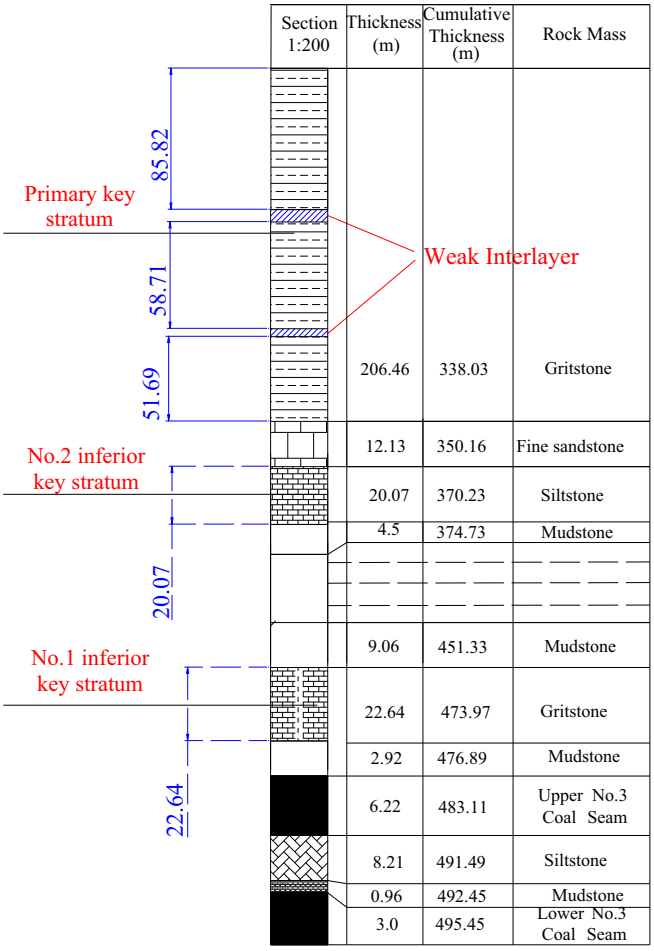

Fig. 4. Synthesis column of Borehole 99-1.

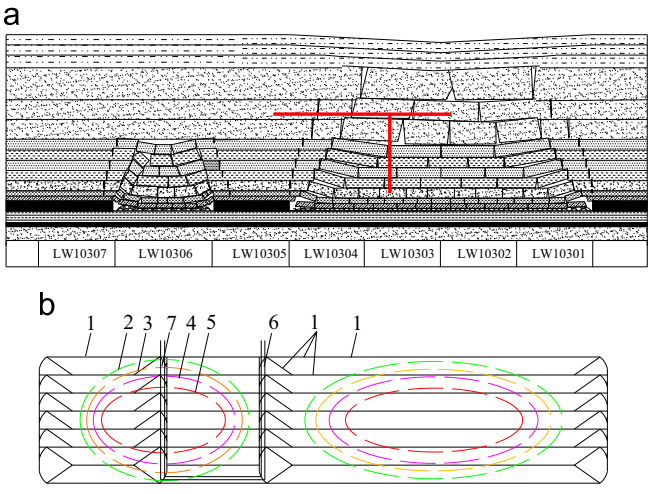

Fig. 5. Sketch of overburden structure above LW10305: (a) overburden structure in the vertical section and (b) overburden structure in the plan view: 1—fracture line of No. 1 inferior key strata; 2—fracture line of No. 2 inferior key strata; 3—fracture line of primary key strata (lower slice); 4—fracture line of primary key strata (middle slice); 5—fracture line of primary key strata (upper slice); 6—headentry; and 7—tailentry.

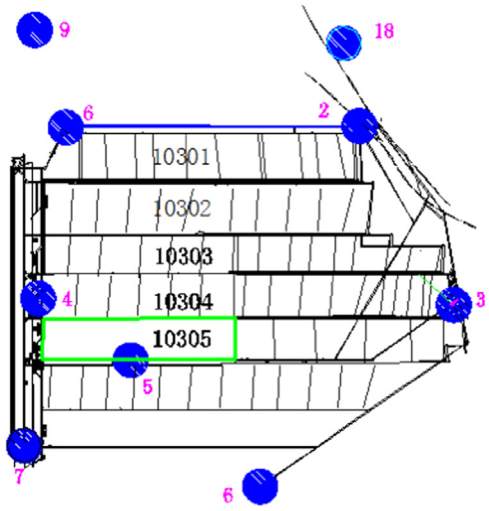

Fig. 6. Layout of geophone stations around Mining District 10 (9# and 18# stations were installed on the surface, while others were installed in underground). (For interpretation of the references to color in this figure, the reader is referred to the web version of this article.)

used to monitor the seismicity around No. 10 Mining District. Data acquisition for passive tomographic imaging during LW10305 mining were conducted with the microseismic monitoring system, which utilizes mining-induced seismic events as the energy sources and measures P-wave arrival times after seismic waves pass through coal-rock mass.

To decrease the grid model size, improve the inversion efficiency, and avoid the inconsistent spatial distribution, the passive velocity tomography on LW10305 was performed using the stations (2#, 3#, 4#, 5#, 6#, 7#, 8#, 9# and 18#) and the seismic events located in the target areas. Moreover, considering that P-wave arrivals of one or more stations may be not clear, the seismic events recorded by over five stations were adopted to avoid creating artificial anomaly in tomograms. Calculations have been made in 8 months intervals from March 2012 to October 2012. Because the layout density of monitoring network around No. 10 Mining District is relatively high, and the seismic activities were quite active during the mining process, the network can provide adequate spatial seismic ray coverage of the entire area of study.

4.2. Inversion parameters

Tomographic imaging mainly depends on the velocity distribution, the source–receiver geometry and density, variable gridding, etc. [39]. The inversion iteration of tomograms in this study was conducted using SIRT, which must have an initial velocity value to perturb the first iteration. The initial velocity model allows the inversion and source locations to be more efficiently and accurately calculated. In the process of SIRT solving, event locations were recalculated and the slowness in each cell with regards to all the passing rays was modified once per cycle [39]. Above steps were repeated until the residual time was less than an acceptable amount or the iterative number reached the threshold value. The source–receiver geometry and density will also affect the source location accuracy, and determine how well the ray coverage will be. The variable gridding determines the resolution of seismic tomography, i.e., allows areas that are not well sampled to be adequately constrained [40].

In this study, considering that the strike (in the X direction) and inclined (in the Y direction) lengths of No. 10 Mining District are about 2 km and 1.5 km, respectively, and the mining depth (in the Z direction) of No. 3 Coal Seam is about 480 m ($Z=-450$ m), to ensure the seismic ray density can satisfy inversion requirement,

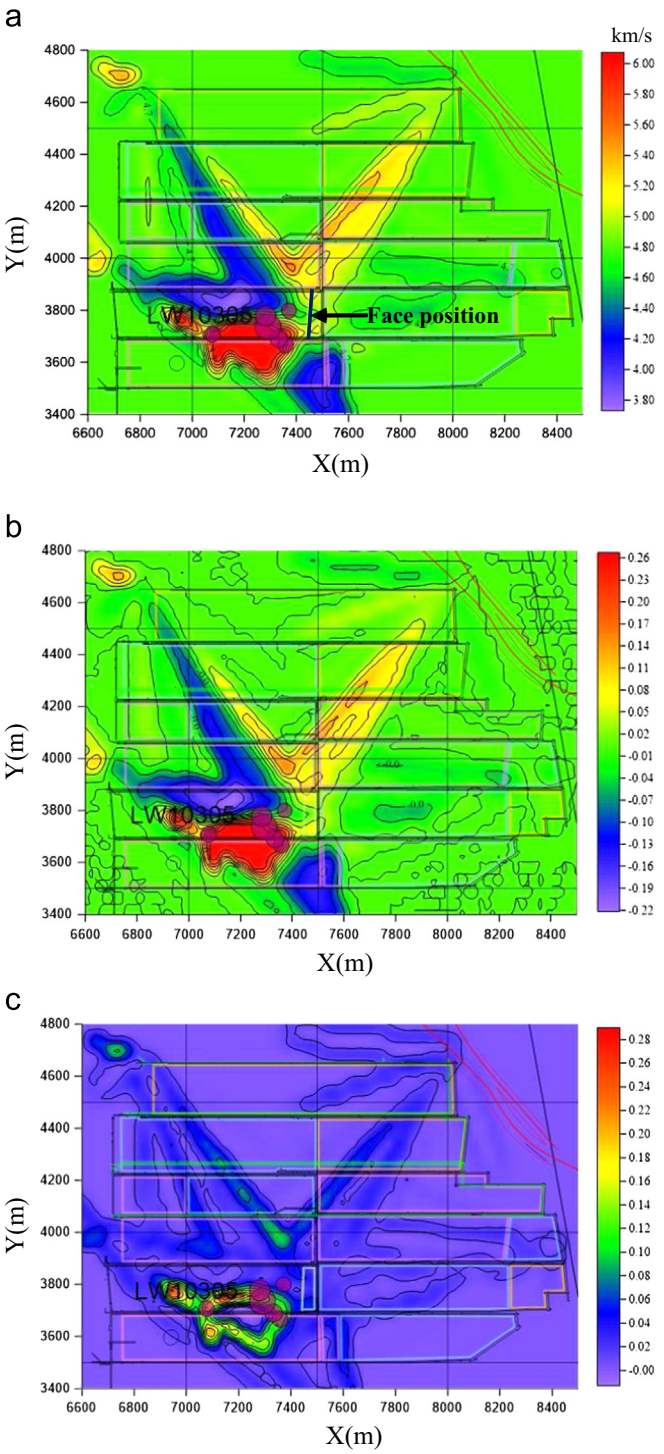

Fig. 7. Tomography images obtained using seismic events from 5 to 31 March (circle symbols show positions of strong tremors with energies $E>10^4$ J that occurred between 1 and 30 April): (a) velocity inversion result; (b) velocity anomaly inversion result; and (c) velocity gradient anomaly inversion result.

and improve the computational efficiency, total $71\times61\times5$ voxel points, with each voxel size of 30 m × 30 m × 125 m in the X, Y, Z directions, respectively, were input into for tomographic calculation. A layer initial velocity model in calculation was assumed in the investigation area, based on geophysical data that has been previously collected, while the constant P-wave velocity equal to 4.1 km/s was assumed to calculate the seismic event location and perturb the first iteration. To reduce the indeterminacy, the velocity was restricted in constant gradient between 2.0 and

6.0 km/s. In addition, the ray-tracing method used for velocity calculation is the hybrid algorithm combined with shortest path method and ray bending method.

4.3. Tomography results and discussion

Plan views of velocity tomograms at the seam level, $Z=-430$ m, were generated for each month, to investigate high seismic activity zones and evaluate seismic hazard risk for the next mining period.

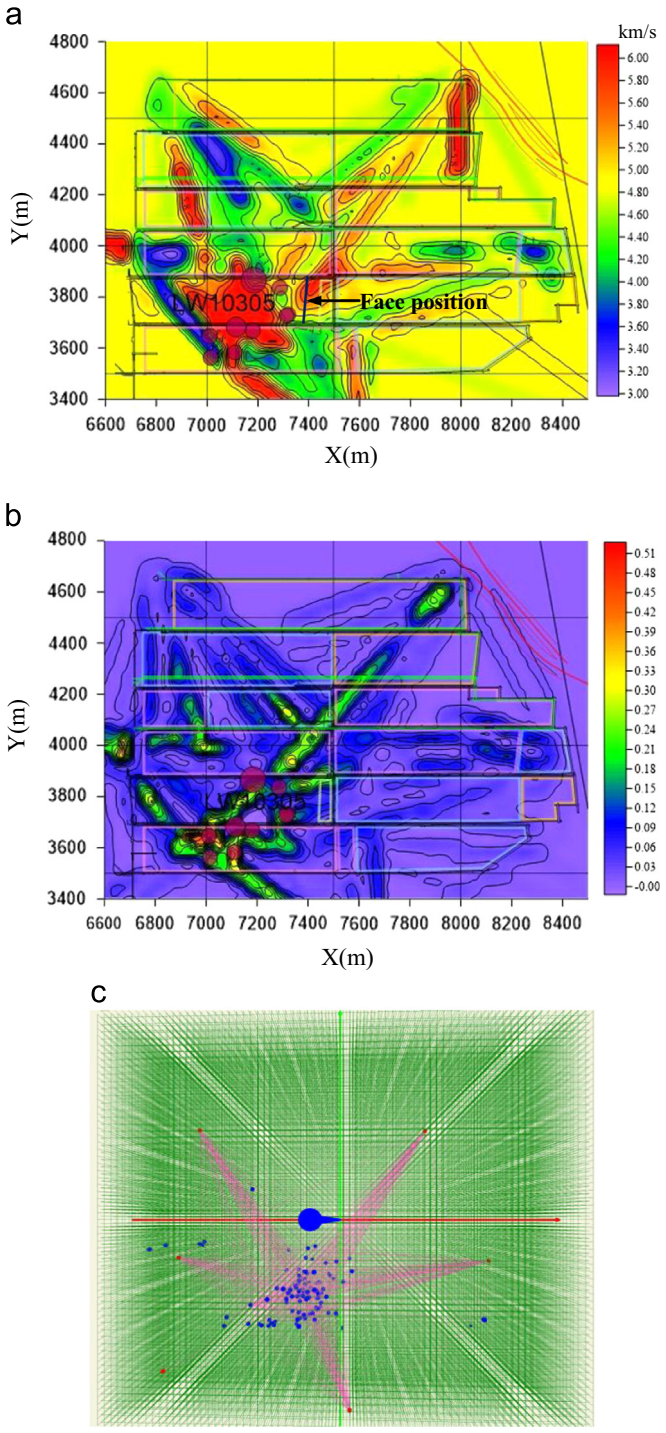

Fig. 8. Tomography images obtained using seismic events between 1 and 30 April (circle symbols show positions of strong tremors with energies $E>10^4$ J that occurred between 1 and 31 May): (a) velocity inversion result; (b) velocity gradient anomaly inversion result; and (c) plan view of P-wave ray paths of events occurred in April.

(1) *5–31 March, 2012*: Mining operation in LW10305 was started on 5 March, and completed on 21 October, 2012. The face was retreated about 48 m at the end of March. In this period, over 645 events associated with roof and floor breakages were recorded, while 105 seismic events were selected for passive tomographic imaging because each of them were recorded and located by over five geophone stations. Calculated velocity image and velocity gradient image are shown in Fig. 7. High velocity and velocity gradient anomaly were observed near the tailgate side ahead of LW10305 and the goafing area of LW10306. The maximum value of P-wave velocity is up to 5700 m/s, while the maximum positive anomalies of velocity and velocity gradient are 0.23 and 0.21, respectively, which indicates that the areas mentioned above were at a middle seismic hazard risk at present stage and in the further mining period, due to the rupture or movement of overburden above LW10305 and LW10306.
Seven tremors with seismic energy over 10^4 J were recorded between 1 April and 30 April. As shown in Fig. 7, the strong tremors located well inside the high velocity area and the area of high velocity gradient. Almost all the strong tremors caused underground strata behaviors and surface transitory shaking to different degrees. Particularly, a strong tremor with energy equal to 8.49×10^6 J occurred about 130 m ahead of the face and near the tailentry on 4 April 2012, inducing serious vibration and obvious strata behaviors in the tailentry. The presented results show that the strong seismic tremors correlate well with the high velocity zones and high velocity gradient zones.

(2) *1–30 April 2012*: LW10305 was retreated about 68 m in April, which means the mining intensity was somewhat increased comparing with the initial mining period. Calculated velocity images are shown in Fig. 8. High velocity or velocity gradient anomaly zone were observed ahead of LW10305, and in the junction of LW10305 and 10306, as well as some partial regions in the sufficiency mining area. According to P-wave ray paths distribution (Fig. 8(c)), high velocity zone observed in the sufficiency mining area is improbable, which indicates the seismic anomaly zones in further time may still locate ahead of LW10305 and near the tailentry, but the anomaly area and seismic risk degree increased obviously.
Nine strong tremors with seismic energy over 10^4 J observed between 1 May and 31 May were plotted to correlate them with high velocity and velocity gradient zones. Almost all the future strong tremors occurred within the credible high velocity or high velocity gradient zones (Fig. 8).

(3) *1 May–31 August, 2012*: Tomographic velocity images in Fig. 9 show further changes of P-wave velocity during the mining period of LW10305 from 1 May to 31 August, 2012. The high-

Fig. 9. Tomography images in each month during the period from 1 May 2012 to 31 August 2012 (circle symbols show positions of strong tremors with energies $E>10^4$ J that occurred in next month of the corresponding velocity inversion): (a) velocity anomaly image using seismic events between 1 and 31 May (high velocity anomaly regions appeared in the intersection area of LW10305 and 10306, near the tailgate side, while the maximum positive velocity anomaly reached to 0.31); (b) velocity anomaly image using seismic events between 1 and 30 June (the credible high velocity regions appeared in the intersection area of LW10305 and 10306, and the protective pillar area, while the maximum positive velocity anomaly was about 0.15); (c) velocity anomaly image using seismic events between 1 and 31 July (high velocity regions mainly appeared near tailgate of LW10305, goafing of LW10306, and the protective pillar area, while the maximum positive velocity anomaly was about 0.20); and (d) velocity anomaly image using seismic events between 1 and 31 August (the credible high velocity regions increased, mainly appeared in the goafing of LW10306 and 10305, and the protective pillar area, while the maximum positive velocity anomaly was about 0.23).

velocity regions were observed to redistribute as LW10305 retreated, from the goafing area of LW10306 to the area ahead of LW10305, and to the protective pillar area of No. 10 Mining District. Moreover, most of the future strong tremors with energy over 10^4 J occurred above LW10305 and 10306, within or near to the relatively high velocity zones.

(4) *1–30 September, 2012*: Calculated velocity image is shown in Fig. 10. As LW10305 retreated towards the stopping line, high velocity and velocity gradient anomaly regions with the middle seismic risk degree, were observed to concentrate near the protective pillar area of No. 10 Mining District, and the intersection area of LW10305, 10306 and 10304, which indicates that there exists large-scale rupture and movement of

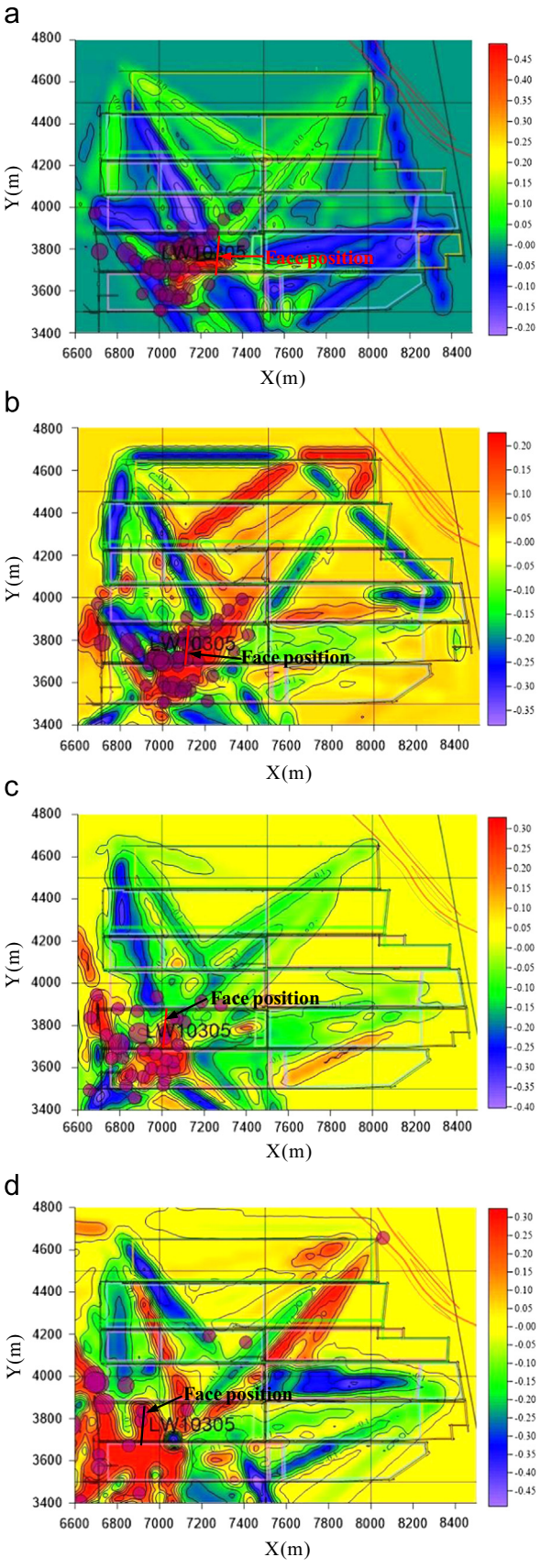

Fig. 10. Tomography images obtained using seismic events between 1 and 30 September (circle symbols show positions of strong tremors with energies > 10^4 J that occurred between 1 and 21 October, 2012); (a) velocity inversion result; (b) velocity gradient inversion result; and (c) plan view of P-wave ray paths of events occurred in September.

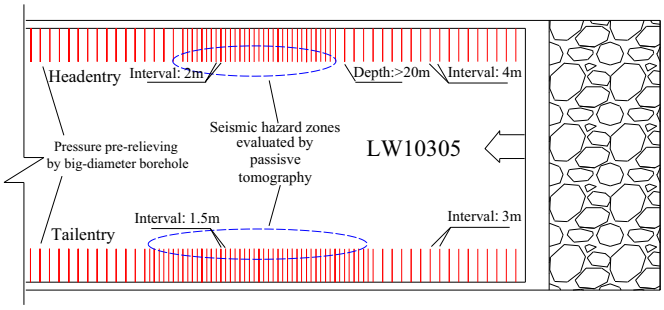

Fig. 11. Schematic diagram of pressure-relief by big-diameter boreholes in LW10305.

overlying strata above the goafing, and causes high stress concentration in the protective coal pillar with the constant increase of mined-out areas. Over 20 strong tremors with energy over 10^4 J were recorded between 1 October and 21 October 2012. Nearly all the strong seismic events were correlated with the credible high velocity and velocity gradient areas, especially occurred in the protective pillar area (Fig. 10).

4.4. Seismic hazard control

Considering the superposition of high static stress around the island face and dynamic load of mining-induced tremors, rock burst risk during the mining operation of LW10305 may be strong. To reduce the static stress level and dynamic disturbance of tremors, pressure pre-relieving in big-diameter boreholes were carried out in tailentry and headentry before LW10305 being mined, seen in Fig. 11. The specified parameters are as follows: borehole diameter is 113 mm, borehole depth is larger than 20 m, borehole intervals are 3 m in tailentry and 4 m in headentry, respectively. In mining process, big-diameter boreholes were supplemented between exiting pre-relieving boreholes in the seismic hazard areas evaluated by velocity tomographic imaging, to reduce stress concentration and seismic hazard risk in advance.

By using above pressure-relief technique, the integrity and intensity of coal mass were destroyed and the static stress was reduced. Moreover, the artificial “loose and weak structure” was formed in coal seam, which can absorb and scatter seismic energies radiated by strong tremors from high-level key strata greatly. During the mining process, 31 strong tremors with energy over 10^5 J occurred. The occurrence of strong tremors always causes buildings on the ground shaking slightly and strata behavior in underground increasing with different degrees. Fortunately, these tremors did not induce serious rock burst accident and cause no injury and loss of life in underground.

5. Conclusions

Before velocity tomography was applied at the field-scale, the relation between stress and wave velocity was examined at the laboratory-scale. It was found that there existed positive exponential correlation between P-wave velocity and applied stress. Combining seismic monitoring and tomography imaging, provides a new method for seismic hazard assessment and pre-warning in underground mining. An island coalface under super-thick strata, LW10305 in Baodian Coal Mine, which may suffer from the threats of strong tremors, was chosen for velocity tomography study in this paper. The case study in LW10305 confirms a good correlation between the areas of high velocity or velocity gradient anomalies and the zones of high seismic activities. Through the tomography detection practice, passive velocity tomography is a promising tool to continuously monitor the relatively high stress or evaluate rock burst hazard in a mine, especially in the being-mined coalface.

Meanwhile, inversion accuracy of passive tomography is mainly affected by the optimal layout of seismic network, establishment of initial velocity model, solution of iterative algorithm, screening of monitoring data, and identification of credible inversion zone, etc. In view of the late development of underground seismic monitoring and complex mining conditions in China, the development and application of passive tomography can improve the seismic monitoring and pre-warning level for strong tremor and rock burst in coal mines.

Furthermore, active tomography, as well as some traditional detection methods, can be applied together with passive tomography, to identify and quantify the results of tomograms. Thus, the seismic tomography in underground coal mines can be improved, contributing to a safer and more productive environment.

Acknowledgments

We gratefully acknowledge the financial support for this work provided by National Natural Science Foundation of China (51204165), National Twelfth Five-year Key Science & Technology Foundation of China (2012BAK04B06), Project of PADD funded by the Priority Academic Program Development of Jiangsu Higher Education Instruction (SZBF2011-6-B35), National Basic Research Program of China (973) (2010CB226805), and Fundamental Research Funds for the Central Universities (2012BZB17).

References

[1] Gibowicz SJ, Kijko A. An introduction to mining seismology. San Diego: Academic Press; 1994. p. 22–3.
[2] He XS, Li SY, Pan K, Zhang TZ, Wang LY, Xu ZH, et al. Mining seismicity, gas outburst and the significance of their relationship in the study of physics of earthquake source. Acta Seismol Sin 2007;20(3):332–47.
[3] Dou LM, Chen TJ, Gong SY, He H, Zhang SB. Rockburst hazard determination by using computed tomography technology in deep workface. Saf Sci 2012;50:736–40.
[4] Cao AY. Research on seismic effort of burst and failure of coal-rock mass associated with mining and its application. China: China University of Mining and Technology; 2009 [Ph.D. thesis].
[5] Li T, Cai MF, Cai M. A review of mining-induced seismicity in China. Int J Rock Mech Min Sci 2007;44:1149–71.
[6] He XQ, Chen WX, Nie BS, Mitri H. Electromagnetic emission theory and its application to dynamic phenomena in coal-rock. Int J Rock Mech Min Sci 2011;48:1352–8.
[7] Wang EY, He XQ, Wei JP, Nie BS, Song DZ. Electromagnetic emission graded warning model and its applications against coal rock dynamic collapses. Int J Rock Mech Min Sci 2011;48:556–64.
[8] Gu S, Wang C, Jiang B, Tan Y, Li N. Field test of rock burst danger based on drilling pulverized coal parameters. Disaster Adv 2012;5:237–40.
[9] Qi QX, Li SB, Wang SK. Application of AE technique in monitoring ground pressure. J China Coal Soc 1994;19(3):221–32.
[10] Qu XC, Jiang FX, Yu ZX. Rockburst monitoring and precaution technology based on equivalent drilling research and its application. China J Rock Mech Eng 2011;30(11):2346–51.
[11] Zhang N, Zhang NC, Han CL, Qian DY, Xue F. Borehole stress monitoring analysis on advanced abutment pressure induced by Longwall Mining. Arab J Geosci 2014;7:457–63.
[12] Jiang FX, Yang SH, Cheng YH, Zhang XM, Mao ZY, Xu FJ. A study on microseismic monitoring of rock burst in coal mine. Chin J Geophys 2006;49(5):1511–6.
[13] Zhao YG, Li Q, Guo H, Jin HX, Wang CF. Seismic attenuation tomography in frequency domain and its application to engineering. Sci China (Ser D) 2000;43(4):431–8.
[14] Luxbacher K, Westman E, Swanson P, Karfakis M. Three-dimensional time-lapse velocity tomography of an underground longwall panel. Int J Rock Mech Min Sci 2008;45(4):478–85.
[15] He H, Dou LM, Li XW, Qiao QQ, Chen TJ, Gong SY. Active velocity tomography for assessing rock burst hazards in a kilometer deep mine. Min Sci Technol 2011;21:673–6.

[16] Friedel MJ, Jackson MJ, Scott DF, Williams TJ, Olson MS. 3-D tomographic imaging of anomalous conditions in a deep silver mine. J Appl Geophys 1995;34:1–21.
[17] Friedel MJ, Scott DF, Williams TJ. Temporal imaging of mine-induced stress change using seismic tomography. Eng Geol 1997;46:131–41.
[18] Luo X, King A, Van de Werken M. Tomographic imaging of rock conditions ahead of mining using the shearer as a seismic source—a feasibility study. IEEE Trans Geosci Remote Sensing 2009;47:3671–8.
[19] Lurka A. Location of high seismic activity zones and seismic hazard assessment in Zabrze Bielszowice coal mine using passive tomography. Chin Univ Min Technol 2008;18:177–81.
[20] Banka P, Jaworski A. Possibility of more precise analytical prediction of rock mass energy changes with the use of passive seismic tomography readings. Arch Min Sci 2010;55:723–31.
[21] Glazer S, Lurka A. Application of passive seismic tomography to cave mining operations based on experience at Palabora Mining Company, South Africa. In: Proceedings of 1st international symposium on block and sub-level caving. Cape Town, South Africa; 2007. p. 369–88.
[22] Hosseini N, Oraee K, Shahriar K, Goshtasbi K. Studying the stress redistribution around the longwall mining panel using passive seismic velocity tomography and geostatistical estimation. Arab J Geosci 2013;6:1407–16.
[23] Westman E, Luxbacher K, Schafrik S. Passive seismic tomography for three-dimensional time-lapse imaging of mining-induced rock mass changes. Lead Edge 2012;31:338–45.
[24] Hosseini N, Oraee K, Shahriar K, Goshtasbi K. Passive seismic velocity tomography and geostatistical simulation on longwall ming panel. Arch Min Sci 2012;57:139–55.
[25] Peng SP, Ling BC, Liu SD. Application of seismic tomography in longwall top-coal caving face. Chin J Rock Mech Eng 2002;21(12):1786–90.
[26] Scott DF, Williams TJ, Tesarik D, Denton DK, Knoll SJ, Jordan J. Geophysical methods to detect stress in underground mines. Report of investigations RI9661. US Department of Health and Human Services; 2004. ⟨http://www.cdc.gov/niosh/mining/UserFiles/works/pdfs/RI9661.pdf⟩.
[27] Westman E, Haramy K, Rock A. Seismic tomography for longwall stress analysis. Rock mechanics tools and techniques 1996:397–403.
[28 Gong SY. Research and application of using mine tremor velocity tomography to forecast rockburst danger in coal mine. China: China University of Mining and Technology; 2010 [Ph.D. thesis].
[29] Pei SP, Chen YJ, Feng BA, Gao X, Su JR. High-resolution seismic velocity structure and azimuthal anisotropy around the 2010 Ms=7.1 Yushu earthquake, Qinghai, China from 2D tomography. Tectonophysics 2013;584:144–51.
[30] Zhang FX, Wu QJ, Li YH. The traveltime tomography study by teleseismic P wave data in the Northeast China area. Chin J Geophys 2013;56:2690–700.
[31] Stanton A. Wilhelm Conrad Röntgen on a new kind of rays: translation of a paper read before the Würzburg Physical and Medical Society, 1895. Nature 1896; 53: 274-276.
[32] Dines KA, Lytle RJ. Computerized geophysical tomography. Proc IEEE 1979;67:1065–73.
[33] Adams L, Williamson E. On the compressibility of minerals and rocks at high pressures. J Frankl Inst 1923;195:475–531.
[34] Yale D. Recent advances in rock physics. Geophysics 1985;50(12):2480–91.
[35] Zimmerman RW, King MS. Propagation of acoustic waves through a cracked rock. In: Proceedings of the 26th U.S. symposium on rock mechanics. Rapid City, SD; 1985. p. 739–45.
[36] Hopkins DL, Cook NGW, Myer LR. Normal joint stiffness as a function of spatial geometry and surface roughness. In: Barton N, Stephansson O, editors. Rock joints. Rotterdam: Balkema; 1990. p. 203–10.
[37] Dou LM, He XQ. Mining geophysics. Beijing: China Science and Culture Press; 2002. p. 152.
[38] Dou LM, He XQ, He H, He J, Fan J. Spatial structure evolution of overlying strata and inducing mechanism of rockburst in coal mine. Trans Nonferrous Metals Soc China 2014;24:1255–61.
[39] Hosseini N, Oraee K, Shahriar K, Goshtasbi K. Passive seismic velocity tomography on longwall mining panel based on simultaneous iterative reconstructive technique (SIRT). J Central South Univ 2012;19:2297–306.
[40] Williamson P. A guide to the limits of resolution imposed by scattering in ray tomography. Geophysics 1991;56:202–7.